Interaction of reactive ions with Pt(100). I. Neutralization and surface trapping

Housei Akazawa and Yoshitada Murata

Citation: The Journal of Chemical Physics **92**, 5551 (1990); doi: 10.1063/1.458488
View online: http://dx.doi.org/10.1063/1.458488
View Table of Contents: http://scitation.aip.org/content/aip/journal/jcp/92/9?ver=pdfcov
Published by the AIP Publishing

Interaction of reactive ions with Pt(100). I. Neutralization and surface trapping

Housei Akazawa[a] and Yoshitada Murata
The Institute for Solid State Physics, The University of Tokyo, 7-22-1, Roppongi, Minato-ku, Tokyo 106, Japan

(Received 30 March 1989; accepted 11 January 1990)

Scattering of (10–400 eV) O^+, O_2^+, C^+, CO^+, and CO_2^+ ions from a Pt(100) surface has been studied. Below 100 eV, the peak position of the angular distribution for survival ions was shifted parallel to the surface, and the lobe width was very narrow in comparison with noble-gas ions. This suggests that surface trapping due to chemical interaction takes place at very low energies. The importance of collisional neutralization at high energies is demonstrated by the result that the yields of reactive ions decrease steeply with increasing incident energy. The scattering ion yields of O^+ and O_2^+ ions, especially, were very low, being less than 1/100 and 1/10 of those of nitrogen ions, respectively. These results show that a chemical interaction effect is significant for the scattering of oxygen ions.

I. INTRODUCTION

A study of the dymanics of atoms, molecules, and ions on solid surfaces is of great importance in order to understand various microscopic surface processes. This study has been made possible by the development of beam techniques and detection systems as well as other experimental methods for characterizing surfaces. Figure 1 shows the relevant energy region for studies that use ion and molecular beams in surface science. The indicated phenomena are characteristic of the corresponding beam energy. Not all of them have yet been observed directly, but they are expected to be observed in the future. Previously the ion and molecular beams have been employed for different purposes and have been developed separately.

Ion-surface scattering covers a wide energy range, since ions are easily accelerated by an electrostatic field. Generally, this phenomenon is divided into three types depending on the incident energy: high-energy ion scattering (HEIS), medium-energy ion scattering (MEIS), and low-energy ion scattering (LEIS). With a high-energy beam, various quantitative analyses such as particle-induced x-ray emission (PIXE), elastic recoil detection analysis (ERDA), and nuclear reactions are known. Modification of the surface region by implantation is also important for technology. MEIS is used to accurately determine surface structures,[1] while LEIS is used to clarify elementary surface compositions as ion scattering spectroscopy (ISS)[2,3] and to analyze surface structures. In a standard experiment of low-energy ion-surface scattering the lower limit of the beam energy is 100–200 eV. If the energy is lowered below 100 eV, the ion beam is defocused and the beam intensity decreases abruptly due to the space-charge effect. Therefore, there have been very few experiments reported using ion beams of less than 100 eV, except for alkali-metal ion beams. Actually the only dynamic phenomena which have attracted interest so far in the low-energy region are ion neutralization and dissociative scattering of molecular ions, although the latter has been a minor topic for a limited number of groups.

In contrast to the low-energy ion beams, monochromatized molecular beams have been applied extensively to study gas-surface interaction and chemical reaction on surfaces.[4,5] The kinetic energy of a seeded molecular beam produced from a supersonic nozzle is usually limited to less than 4 eV for light diatomic molecules such as H_2, O_2, N_2, and NO, while I_2 molecules can be accelerated to about 10 eV.[6,7] Molecular beam scattering from surfaces (direct inelastic scattering, trapping desorption, and resonance scattering) provides information on the nature of interaction potentials, energy exchange, or other inelastic interactions. By a study of selective adsorption or activated dissociative adsorption, the depth of an attractive well on the surface can be probed.

Actually, gas (ion)-surface interactions have been unremarked in the region from a few to 100 eV. Very few experiments have been performed with these energies due to the difficulty in beam production and in efficiently detecting scattered ions (neutrals). Recently, however, there has been growing interest in this intermediate energy region, both experimentally and theoretically. In principle, both ion and molecular beams have the potential for application to a study in the 1–100 eV region, if experimental difficulties are resolved. Dynamic studies using a combination of both ion and molecular beams are now capable of implementation. As a result many formerly unexplored phenomena charac-

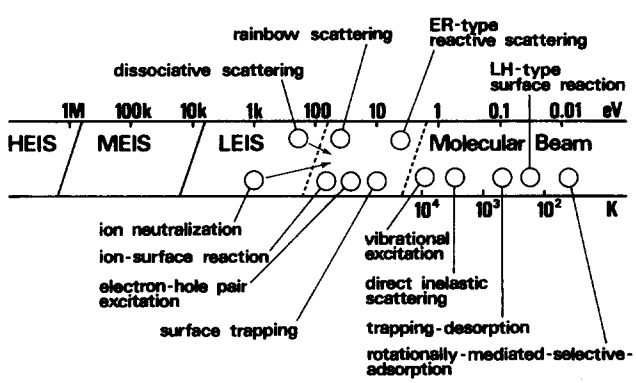

FIG. 1. Energy regions relevant to a study of surface science using ion and molecular beams. Typical dynamic phenomena that are characteristic of the corresponding beam energy are also indicated.

[a] Present address: NTT LSI Laboratories, 3-1, Morinosato Wakamiya, Atsugi 243-01, Japan

 0021-9606/90/095551-09$03.00

teristic of this energy region can be verified. The 1–10 eV region is called the chemical region, since the chemical bond energy of a molecule is about a few eV. This means that most ion-surface scattering experiments have so far been carried out at energies too high to investigate the chemical process. If it can be assumed that ion-surface interaction is scaled by normal energy (the normal component of the kinetic energy with respect to the surface), a condition satisfying (1–10 eV) normal energy is easily obtained by the grazing incidence of a low-energy ion beam.[8,9] However, this assumption seems to be valid only as special cases.

From the viewpoint of projectile-surface interaction potential, the energy of 1–100 eV is a difficult intermediate region. When a typical energy for LEIS (above 100 eV) is used, the scattering process is generally treated as a series of binary collisions with target atoms.[10] A pairwise interaction potential can be used to describe the collision process. In the opposite extreme, i.e., thermal-energy neutral-beam scattering, the surface cannot be treated as an arrangement of individual surface atoms. Even diffraction is observed due to collective interaction with the potential hypersurface. With increasing beam energy, the surface is first seen by a projectile as a flat hard wall, then as a flat soft wall at 1–10 eV, and as a spherically corrugated surface at 10–100 eV. In the 10–100 eV region, surface rainbow scattering is observed by using an alkali-metal ion (neutral) projectile with a medium angle of incidence.[11,12] The surface structure is reflected by the energy spectra and by the angular distributions of the scattering particles.

Various dynamic processes in the 1–100 eV region are described in Fig. 1. Chemical bond breaking of the projectile molecule is observed either in activated dissociative chemisorption or in dissociative scattering. The former can be regarded as a kind of ion-surface reaction.

An important inelastic effect comes into play in this energy region. Energy dissipation of the projectile is mainly due to phonon excitation if the beam energy is in the thermal region and if the projectile mass is lower than that of the target atom. If the projectile is more massive than the target atom, another mechanism of energy dissipation is open, i.e., an electron–hole pair is excited.[13] Such an energy transfer is frequently coupled with the internal degrees of freedom of an incident molecule, because vibrational excitation and ion emission are expected to occur.

In the usual theoretical treatment of ion-surface scattering processes, attractive interactions such as image charge interaction are neglected. However, if the beam energy is lowered and if the projectile can be chemisorbed on the surface, an attractive chemisorption potential should be taken into account.[14] In the scattering trajectory, the projectile enters a chemisorption interaction region and normal energy will be dissipated. If the energy loss is large, the projectile may be trapped temporarily in an attractive well with depth of a few eV while moving along the surface.

Up to now it has been standard knowledge that almost all chemical surface reactions proceed via a Langmuir–Hinshelwood mechanism,[5,15] i.e., a reaction between adsorbates. However, with hyperthermal beam energy, the incident molecule is translationally activated and accommodation to the surface is insufficient during scattering. It is highly probable that the reaction proceeds by another path, i.e., via the Eley–Rideal mechanism.[16–18] This is a direct reaction pathway between an adsorbate and an incoming molecule from the vacuum or a nonthermalized precursor molecule. By using a projectile with a few eV energy, such a nonadiabatic chemical reaction on surfaces could become possible and should be challenged experimentally.

Charge exchange (neutralization and reionization)

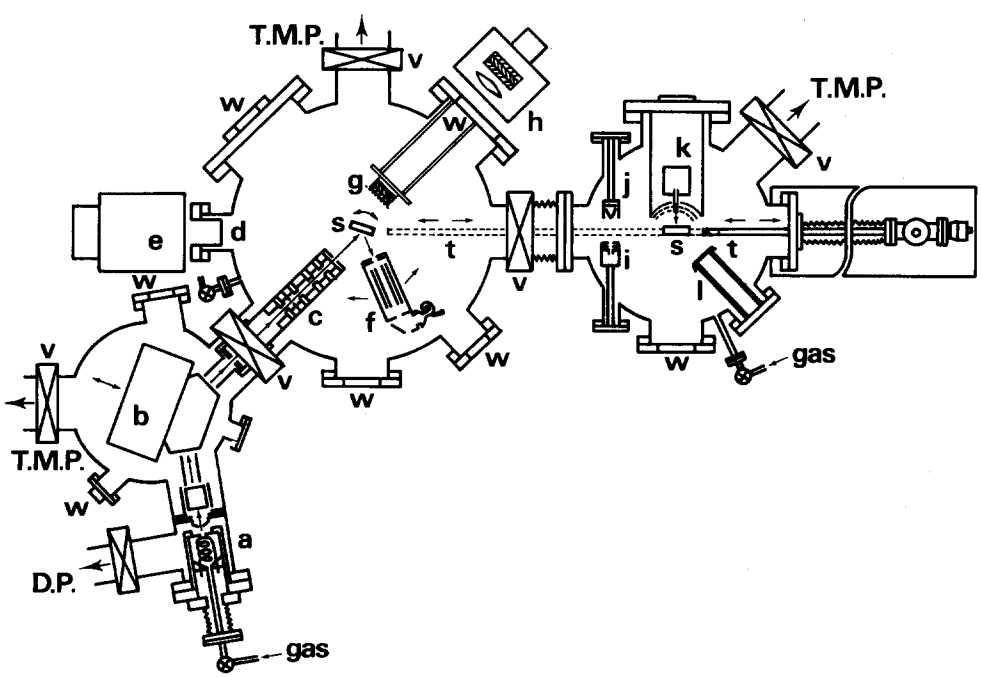

FIG. 2. Schematic representation of the complete apparatus composed of (a) ion source, (b) mass selection magnet, (c) deceleration lens system, (d) quartz window, (e) optical spectrometer, (f) quadrupole mass filter, (g) MCP and fluorescent screen, (h) two-dimensional position-sensitive detector with photocathode and image intensifier, (i) ion sputtering gun, (j) electron bombardment gun, (k) LEED-AES optics, (l) SAES alkali source, (s) sample, (t) sample transfer system, (v) separate valves, and (w) viewing ports.

between noble-gas ions and solid surfaces has been studied extensively. In contrast, ions of chemically reactive species have scarcely been used in such studies. The present paper reports on the scattering of (10–400 eV) reactive ions (O^+, O_2^+, C^+, CO^+, and CO_2^+) from a Pt(100) surface in comparison with that of nonreactive ions. In particular, attention is focused on the study of neutralization and surface trapping due to the incident-energy dependence of the scattered ion yield and the angular distribution.

II. EXPERIMENT

The experimental apparatus is schematically shown in Fig. 2. It consists of four separated chambers: a sample preparation chamber, an ion source chamber, a mass separation chamber, and a scattering chamber. The ion source and mass separation chambers are connected through a 0.5-mm-diam aperture in an extraction lens. The ion source chamber is evacuated by a diffusion pump with a liquid-nitrogen cold trap, and the other chamber is evacuated by a turbomolecular pump, a sputter ion pump, and a Ti-getter pump. The sample preparation chamber is equipped with an electron bombardment gun and an ion sputtering gun for surface cleaning and low-energy electron diffraction (LEED) Auger electron spectroscopy (AES) optics to check the surface structure and the surface cleanliness. The sample is transferred between the preparation and scattering chambers.

The ion beam line has been briefly described elsewhere.[19] The ion source is the Menzinger-type plasma source.[20] Filament current is automatically regulated. Anode voltage is set between 50–150 V, and a 100–200 mA arc current was obtained. Beam current fluctuation on the target is kept within 5% for a few hours. Ions in the source are extracted by accelerating their kinetic energy to about 600 eV and are mass selected. Neutral species are excluded by bending the trajectory with an electromagnet, which is installed in the ultrahigh vacuum (UHV) chamber. The electromagnetic coil is made of a copper pipe wrapped with glass wool and is internally cooled by flowing water. Finally, the ions are successively decelerated by passing through a deceleration lens system until they reach the desired impact energy. An ion source filament, a Mo anode, and an extraction lens are floated from the ground and the incident ion energy is determined by the potential difference between the anode and the grounded sample which is mounted in a field-free region of the ground potential.

The pressure of the gas introduced into the source ranged between 0.05 and 0.2 Torr. The operating pressures in the ion source chamber and in the mass-separation chamber were 10^{-4}–10^{-5} and 10^{-7}–10^{-8} Torr, respectively. Typical operating pressure in the scattering chamber was 1–2×10^{-9} Torr. CO_2 gas was introduced into the ion source to generate C^+, O^+, CO^+, and CO_2^+ ion beams. The ratios of ion species produced were 7% C^+, 3% O^+, 70% CO^+, and 20% CO_2^+. O_2 gas was introduced to generate an O_2^+ ion beam. Since ambient CO_2 was known not to be chemisorbed on the Pt surface at room temperature, it was not necessary to consider the effect of the CO_2 background atmosphere on the scattering process. The sticking coefficient of O_2 is also known to be small on a 5×20 reconstructed Pt(100) surface.[21,22] The ion current obtained on the target surface ranged between 0.3 and 20 nA in the 1–100 eV primary energies. The current was strongly dependent on the ion species and the beam energy.

Scattered ions were detected with a quadrupole mass filter which was rotatable around two axes without energy analysis. Measurement was performed within the in-plane scattering. The acceptance angle by the entrance aperture of the detector was 4°. The mass filter was controlled by a high-power system (Extra-nuclear model 011-1) and the fast ion masses were separated by high transmittance but with poor resolution. The transmitted ion trajectories were bent 90° by using a deflector before detection with an electron multiplier in order to remove neutral species and low-energy secondary ions. After proper cleaning procedures, however, very little secondary-ion emission, except for (directly recoiled) H^+ ions, was observed. The normalized scattering ion yield was obtained by integration of the mass peak and by correction for the mass peak width ΔM. The major advantages to detect ions with very low energy ($E_i \leqslant 100$ eV) by a mass filter instead of an energy analyzer are high transmittance and unambiguous separation of scattered ions from sputtered or recoiled ions.

A Pt single crystal oriented by x-ray diffraction was cut parallel to the (100) lattice plane and was polished with diamond paste down to 1/4 μm. The sample surface was cleaned by repetitive Ar^+ sputtering, annealing in an O_2 atmosphere at a 10^{-6} Torr range at 900 °C, and annealing in a vacuum at 1200 °C. Surface cleanliness was monitored by AES, and a clear 5×20 pattern was observed by LEED.

In molecular-ion incidence, dissociatively scattered ion products were observed in addition to nondissociatively scattered parent ions. In the CO^+ incidence, C^+ was observed. In the CO_2^+ incidence, CO^+ was observed. Details of this dissociative scattering will be reported in the next paper,[23] since the present paper is focused on neutralization and trapping of the parent ions.

III. RESULTS AND DISCUSSION

A. Noble gas versus reactive ones

Positive-ion yields in reactive-ion scattering on metal surfaces are known to be very low in the ordinary energy range of ISS.[8] The energy spectrum for reactive ions has a broad tail that extends to the lower energy. This suggests that projectiles which suffer substantial energy loss emerge as ions. In contrast, the ion yields of noble-gas ions are larger (ion survival probabilities of about 10^{-2}), and usually the energy spectrum shows a sharp elastic peak. These features show intrinsic differences between noble-gas and reactive ions.

Figure 3 shows a schematic description of the charge exchange processes between an ion and a metal surface. The region of ion-surface interaction is usually divided into three parts: incoming trajectory, collisional region, and outgoing trajectory. Resonance neutralization (RN), Auger neutralization (AN), and Auger de-excitation (AD) take place on the incoming and the outgoing trajectory.[24] Collisional neu-

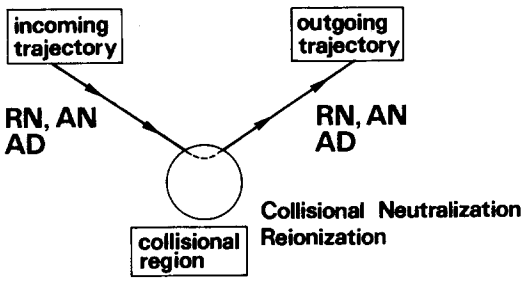

FIG. 3. Schematic representation of the neutralization and deexcitation processes of ions in the surface vicinity and in the collisional region. RN, AN, and AD mean resonance neutralization, Auger neutralization, and Auger de-excitation, respectively.

tralization[25] and reionization[26] are atomic-like processes. They take place when the projectile approaches the target atom close enough to cause overlapping of their wave functions. When a close projectile-target atom encounter occurs, a quasimolecule is formed, and electrons can be transferred. Charge exchange takes place at the diabatic crossing of the energy levels.

Figure 4 shows the energy diagram relevant to neutralization of O^+, O_2^+, C^+, CO^+, and CO_2^+ ions on a Pt surface involving the Pt valence band.[27-29] If the projectile has electronically excited states that are in resonance with the Pt valence band, RN can occur. However, transition to the ground state is considered to be the most dominant process of neutralization, since AN is possible for every state. This energy diagram can account for the electronic transition between the projectile and the surface only, other factors such as chemical effects being beyond the scope of this diagram.

Two significant differences in neutralization exist for noble-gas and reactive ions. One is that electronically excited species are generated by RN of the reactive ions, whereas the lowest excited state of noble-gas ions (He^+, Ne^+, and Ar^+) is located above the Fermi level of the Pt metal; therefore, only AN to the ground state is possible for noble-gas ions. Another difference is that there is only one hole in the valence state of noble-gas ions, whereas there are several holes

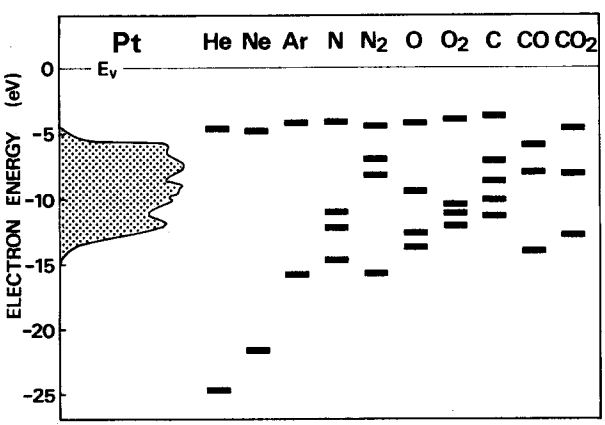

FIG. 4. Energy diagram relevant to the neutralization interpretation of O^+, O_2^+, C^+, CO^+, and CO_2^+ ions on a Pt surface.

for reactive ions. Since the closest approach distance between the projectile ion and the surface becomes shorter as ion energy increases, contributions from collisional neutralization and reionization processes will be smaller than those of RN, AN, and AD processes at very low energies. With increasing energy, collisional process contributions are expected to increase noticeably.

In order to see whether the difference in ion yields and energy spectra of reactive and noble-gas ions is mainly caused by RN or by collisional charge exchange, ion yields of reactive and noble-gas ions are compared at very low energies (10–100 eV). At these energies a small contribution of collisional charge exchange is expected. The ion yields of N^+, N_2^+ (already reported in Ref. 30), CO^+ (Fig. 10), and CO_2^+ (Fig. 11) are comparable with each other, if compared with the same incident energy at θ_i (incidence angle measured from the surface normal) $= \theta_f$ (emission angle measured from the surface normal) $= 70°$ below 100 eV (about 10^4 at 10 eV and about 10^3 at 100 eV in the arbitrary units commonly used). Energy levels of the neutral ground state are located at almost the same position for these projectiles. The ion yields of Ne^+ and Ar^+ are comparable with those of the above four reactive ions below 100 eV.[30,31] This means that the RN process is unimportant in causing the difference of the ion survival probability between reactive and noble-gas ions. Especially, the Ar ground state is located at almost the same energy level as those of the reactive ions. In contrast, at 200–400 eV the ion yields of N^+, N_2^+, CO^+, and CO_2^+ are about 10^2–10^3, whereas those of Ne^+ and Ar^+ are 10^4. From these figures, we can say that the difference in the ion yields between reactive and noble-gas ions mainly originates from the significantly different survival probabilities in the collisional charge exchange process.

B. O^+ and O_2^+ ions

Figures 5 and 6 show scattered O^+ and O_2^+ ion yields as a function of incident energy for two specular scattering geometries. The ion yield is very low. Scattering of positive oxygen ions from a metal surface has seldom been measured. Schubert *et al.*[32] reported a scattering experiment by impinging O_2^+ on Ni(111) at grazing incidence ($\theta_i = \theta_f = 85°$) with energies lower than 1 keV. No surviving positive ions were observed within the sensitivity of the time-of-flight detector. Similarly Haochang *et al.*[33] studied (100–300 eV) O_2^+ scattering from Ag(111). O^+ ion was detected on a lower order of intensity in addition to O_2^- and O^-. Saiki and Tanaka[34] reported that no positive scattered ions were actually detected in O^+ incidence on a polycrystalline Pd surface. Kasi *et al.*[14] reported time-of-flight analysis of scattered particles in (100 and 200 eV)-O^+ incidence on Ni(111) with a scattering angle of 90°. No survival ions were observed. However, these experimental results were carried out using incident ions with energies higher than 100 eV; our results were mainly obtained below 100 eV.

In comparison with the yields of nitrogen ions measured below 100 eV,[30] those of O^+ and O_2^+ are 1/100 and 1/10, respectively. The number of states of the oxygen ion is nearly the same as that of the nitrogen ion, and only the energy

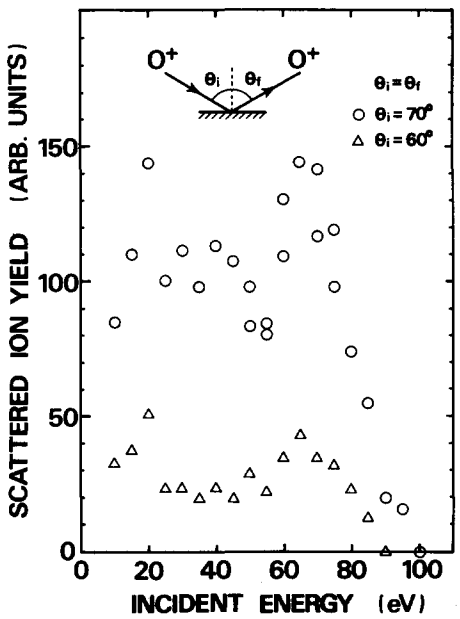

FIG. 5. Incident-energy dependence of the scattered O^+ ion yield for the specular-scattering geometry when $\theta_i = 60$ and 70°.

levels differ slightly. Therefore, it seems impossible to explain the lower ion yields for oxygen ions than those for nitrogen ions and the lower ion yield for O^+ than that for O_2^+ from the energy diagram alone. It was theoretically shown by Hentschke *et al.*[35] that Auger coupling between the projectile state and the valence band of the solid becomes stronger as the energy level of the projectile approaches the band. Then, if one judges from the energy diagram, the ion survival probability of O^+ should be higher than that of O_2^+. However, the opposite is observed.

This may be explained by chemical interactions of oxygen ions with the Pt surface. Oxygen atoms can be chemisorbed on Pt, while nitrogen atoms or molecules cannot be chemisorbed stably on Pt at room temperature. The dissociative chemisorption probability of an oxygen molecule on a 5×20 reconstructed Pt(100) surface is rather low (less than 10^{-3}).[21,22] This suggests that an activation barrier exists in the dissociative chemisorption process for O_2 on a 5×20 reconstructed Pt(100) surface. However, such a barrier can be overcome easily by a hyperthermal energy beam. Part of the scattered O^+ or O_2^+ ions in a direction nearly parallel to the surface may be trapped temporarily on the surface, even if not chemisorbed. As a result, the residence time for oxygen ions in the surface vicinity is expected to be longer than that of nonreactive ions. Then, oxygen ions will have a high neutralization probability and/or a low reflection probability. The result that the ion yield of O_2^+ is ten times as large as that of O^+ may be due to the stronger surface interaction of O^+ than O_2^+, because O^+ is atomic and O_2^+ is molecular.

The angular distributions of scattered O^+ and O_2^+ ions are shown in Figs. 7 and 8, respectively, at an incidence angle of 60°. The lobe is located at 5–10° from the parallel to the surface and the lobe width is very narrow. Ion fraction at large scattering angles decreases and scattered ions are allowed to exit nearly in parallel to the surface. This result suggests that surface trapping of oxygen ions occurs. Snowdon[36] reported an abrupt decrease in the O^- yield below some exit normal energy in O_2^+ incidence on a Ag(111) surface, and the idea of surface trapping was introduced by his experiment.

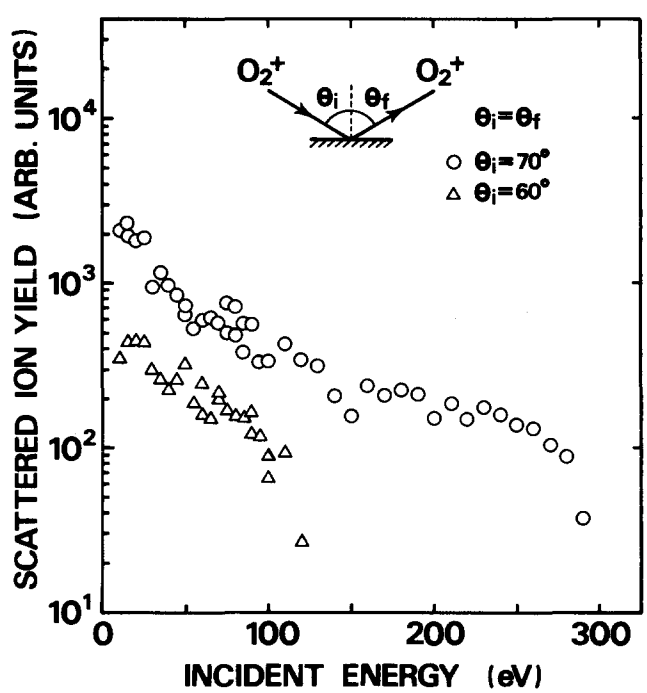

FIG. 6. Incident-energy dependence of the scattered O_2^+ ion yield for the specular-scattering geometry when $\theta_i = 60$ and 70°.

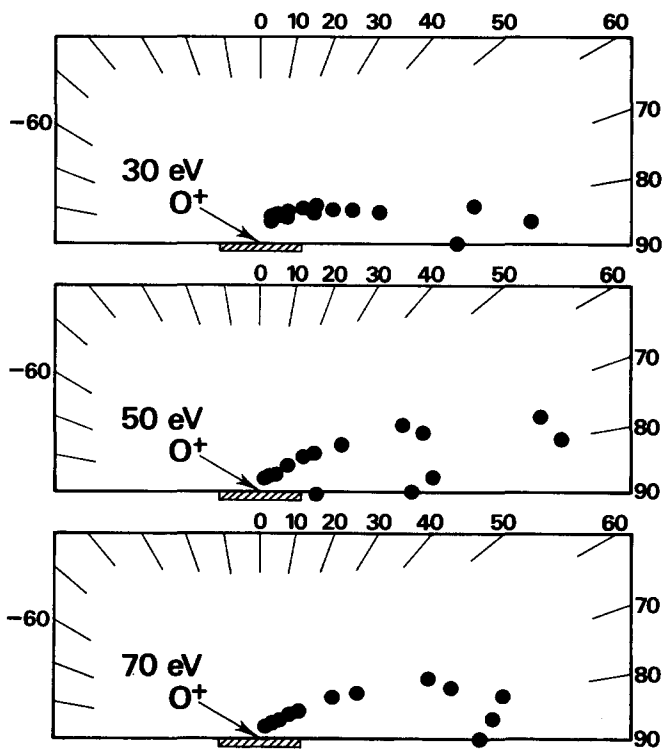

FIG. 7. Angular distributions of scattered O^+ ions at $\theta_i = 60°$ with $E_i = 30$, 50, and 70 eV. The scale is arbitrary.

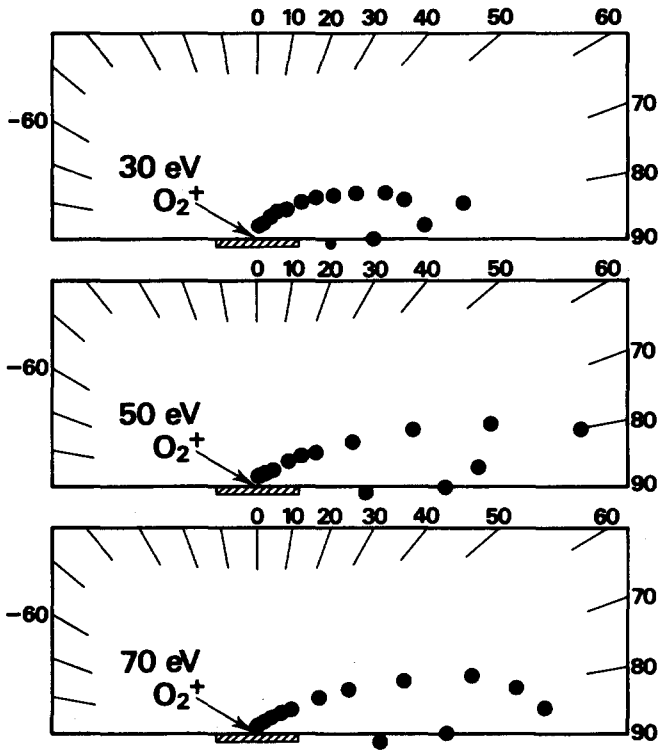

FIG. 8. Angular distributions of scattered O_2^+ ions at $\theta_i = 60°$ with E_i = 30, 50, and 70 eV. The scale is arbitrary.

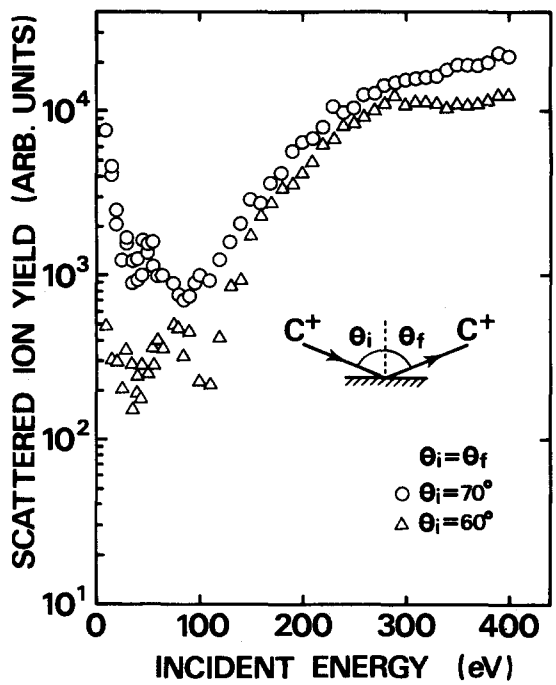

FIG. 9. Incident-energy dependence of the scattered C^+ ion yield for the specular-scattering geometry when $\theta_i = 60$ and 70°.

C. C^+, CO^+, and CO_2^+ ions

Figures 9, 10, and 11 show the scattered ion yields of C^+, CO^+, and CO_2^+, respectively, as a function of incident energy. These yields are larger than those of O^+ and O_2^+ ions. Similar to the results of N_2^+ and O_2^+ ions, a steep decrease in the CO^+ and CO_2^+ ion yields with incident energy was observed. For C^+, a V-shape energy dependence of the yield was observed below 100 eV and the corresponding steep decrease in the yield is seen below 40 eV. This steep decrease can be explained by considering that the transition rate of RN, AN, and especially collisional neutralization increases steeply as ions penetrate deeper into the interaction region of the surface.[30] This can be rationalized by assuming that at very low energies the ion survival probability is determined by the penetration depth of ions into the ion-surface interaction region, rather than the residence time in the surface vicinity. The ion yield of CO_2^+ becomes very low above 100 eV, while that of CO^+ remains constant. The monotonic decrease in the CO_2^+ yield seems to be due to neutralization and dissociation. This occurs because the dissociation of CO_2^+ takes place more efficiently than that of CO^+. The ion yield of CO_2^+ drops from 25 eV with decreasing ion energy. It also indicates trapping of the ions on the surface. The yield of C^+ increases more than one order of magnitude from 100 to 400 eV. This strong increase in the yield seems to be due to an enhanced reionization process, which is similar to ejection of a hydrocarbon, as is well known in secondary-ion mass spectroscopy.

Angular distributions of scattered C^+ and CO^+ are shown in Figs. 12, 13, and 14. Below 100 eV, the lobe position is located at 5–10° from parallel to the surface and the distribution width is narrow. At 200 and 300 eV, the angular distribution of C^+ exhibits a double-peak structure. A similar structure was observed in the angular distribution of Ar^+ with 200–300 eV incident energy.[31] This is explained as a surface rainbow. The peak corresponding to the larger scattering angle originates from a single-collision scattering with

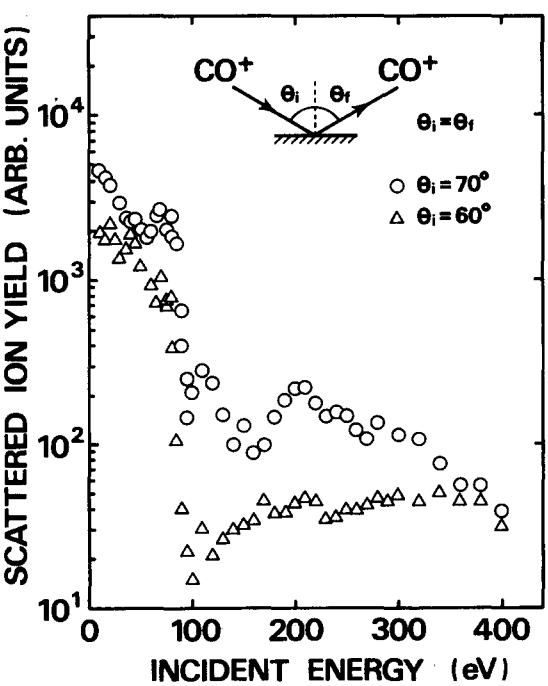

FIG. 10. Incident-energy dependence of the scattered CO^+ ion yield for the specular-scattering geometry when $\theta_i = 60$ and 70°.

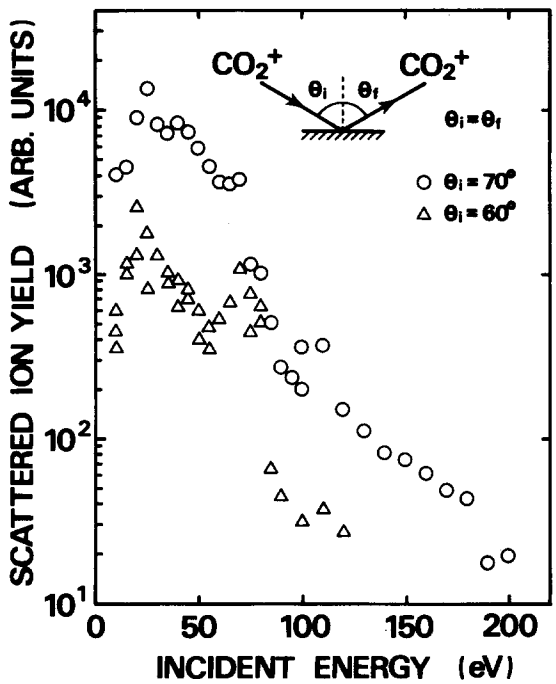

FIG. 11. Incident-energy dependence of the scattered CO_2^+ ion yield for the specular-scattering geometry when $\theta_i = 60$ and 70°.

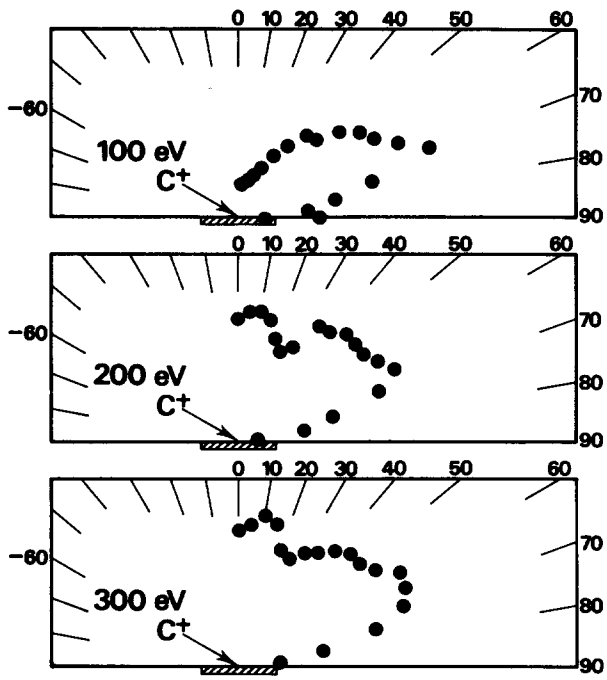

FIG. 13. Angular distributions of scattered C^+ ions at $\theta_i = 60°$ with E_i = 100, 200, and 300 eV. The scale is arbitrary.

a small impact parameter or double-collision scattering. The ion survival probability for such backward scattering is expected to be lower than that for forward scattering with a large impact parameter. Then it can be concluded that the peak of larger scattering angles is due to enhanced reionization. This is consistent with the above discussion. In fact, the energy level of the ground state for a carbon atom (Fig. 4) is 11.3 eV below the vacuum level. This state is located at the

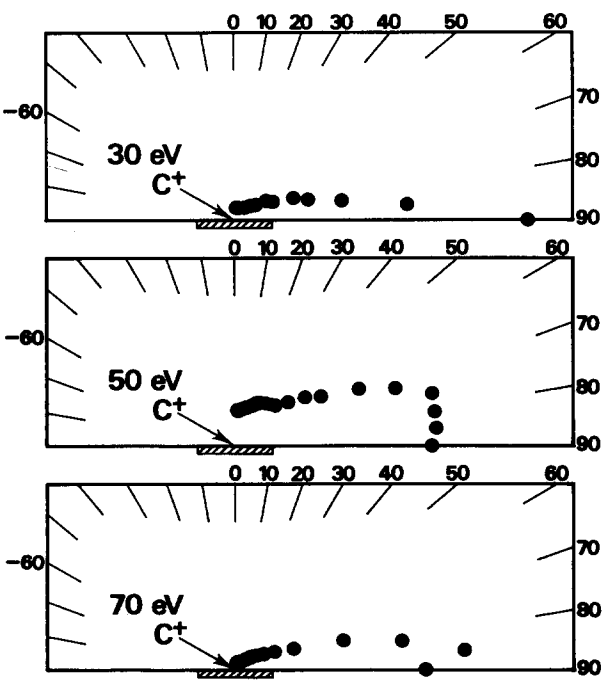

FIG. 12. Angular distributions of scattered C^+ ions at $\theta_i = 60°$ with E_i = 30, 50, and 70 eV. The scale is arbitrary.

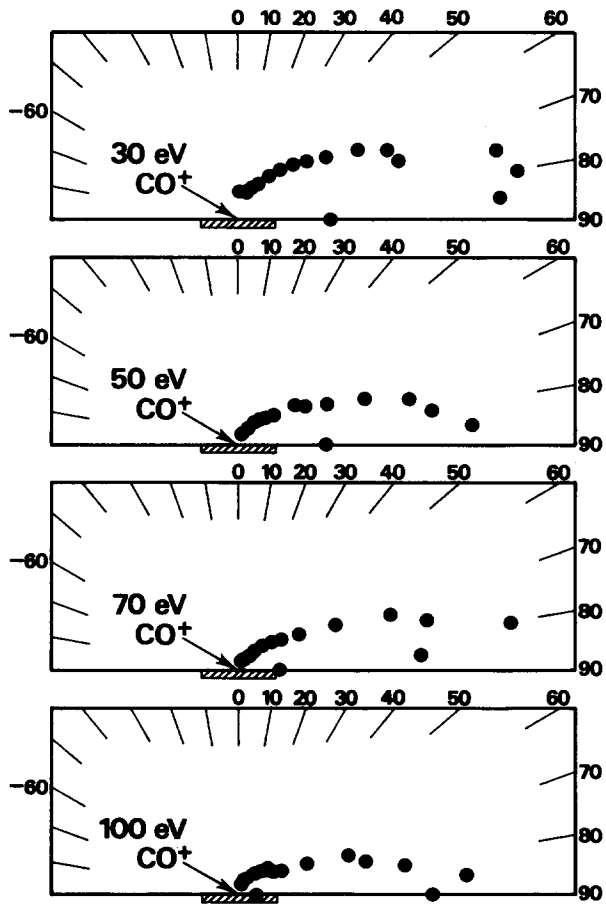

FIG. 14. Angular distributions of scattered CO^+ ions at $\theta_i = 60°$ with E_i = 30, 50, 70, and 100 eV. The scale is arbitrary.

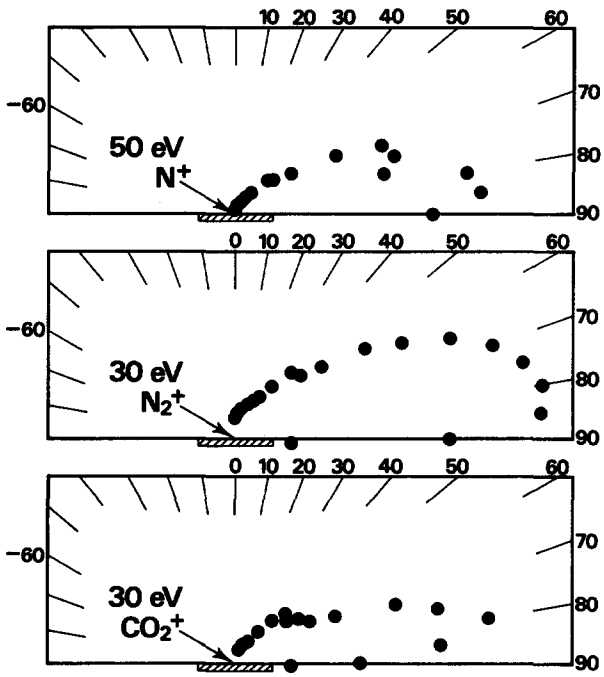

FIG. 15. Angular distributions of scattered ions in 50 eV N^+, 30 eV N_2^+, and 30 eV CO_2^+ incidence. The scale is arbitrary.

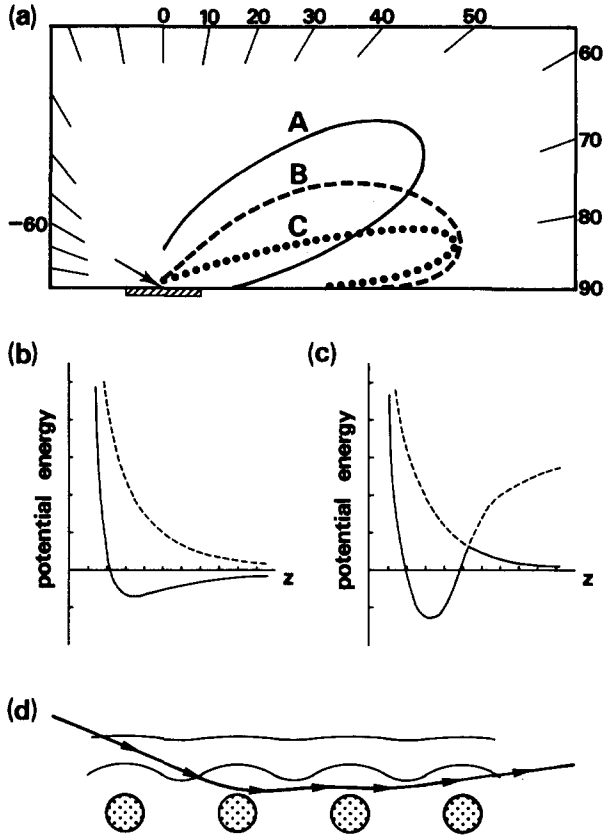

FIG. 16. Schematic representation for explanation of surface trapping and skipping motion. (a) Three types of angular distributions of scattered ions with $E_i = 50$ eV. (b) Ion-surface interaction potential, including image potential. (c) Ion-surface interaction potential with chemisorption interaction. (d) Schematic representation of surface trapping.

highest position of the projectiles shown in Fig. 4 and is completely in resonance with the Pt valence band. Although the ionization energy of the ground state for O_2 is relatively small, most of the O_2^+ ions are expected to be dissociated at energies higher than 100 eV. Therefore, the increase in the O_2^+ yield with increasing energy should not have been observed.

D. Surface trapping of chemically reactive ions

Figure 15 shows supplemental results for the angular distributions of scattered N^+, N_2^+, and CO_2^+ ions at very low energies. Similar to the results of O^+, O_2^+, C^+, and CO^+ incidences at 50 eV, the lobe positions of N^+, N_2^+, and CO_2^+ are located at 5–10° from the parallel to the surface.

There exists a correlation between the exit glancing angle and the angular distribution width for the scattered ions. Scattering of noble-gas ions is characterized by a large exit angle and a wide angular distribution, whereas scattering of the reactive ions is characterized by a small exit angle and a narrow angular distribution. Figure 16(a) shows a comparison between the three types of angular distributions, depending on the projectile species, at an incident energy of 50 eV. The angular distributions of He^+ and Ne^+ show lobes in the specular direction and are classified as type *A*.[31] The angular distribution of Ar^+ belongs to type *B*.[30] The scattering cross section decreases and the inelastic scattering effect becomes significant as the projectile mass increases. Then it is reasonable that the lobe of Ar^+ is located at a smaller scattering angle than those for He^+ and Ne^+. The angular distributions for N_2^+ and N^+ are similar to that for Ar^+. The fact that the lobe position is located at a very small exit angle shows that the blocking effect becomes unimportant at 50 eV. Ions are scattered from shallow potential regions and see a small corrugated surface potential generated by the overlapping of the wave functions for surface atoms. An ion reflected at a small angle will travel along the nearly flat ion-surface interaction potential and will be scattered softly. In type *C*, the lobe position is the same as that of type *B* (5–10° from the surface parallel), but the distribution width is narrower. The angular distributions of O^+, O_2^+, C^+, CO^+, and CO_2^+ are classified into this type. The difference between types *A*, *B*, and *C* may represent the different strengths of the ion-surface interactions with or without the chemisorption force. In fact, the angular distribution of Ne^+ belongs to type *A* and that of C^+ to type *C* despite the comparable masses of Ne^+(10) and C^+(12). Similarly, for Ar^+(40) and CO_2^+(44) the angular distribution of Ar^+ belongs to type *B* and that of CO_2^+ to type *C*. For N_2^+(28) and O_2^+(32), the angular distribution of N_2^+ belongs to type *B* and that of O_2^+ to type *C*. Clearly, the experimental results provide evidence as to the importance of chemical interaction, which is reflected in the angular distribution of scattered ions.

Figures 16(b)–16(d) show an explanation of the surface trapping or the skipping motion of reactive ions. For nonreactive ions, attractive interaction is the image charge interaction only. The repulsive potential is schematically

shown by the broken line in Fig. 16(b) and the total potential, including the attractive interaction, is shown by the solid line. In the case of reactive ions, a minimum of the chemisorption potential exists in the region close to the surface. The adiabatic curve is shown by the solid line in Fig. 16(c). If the ion energy is very low and the incidence angle is large, the surface potential appears to be nearly flat to an incoming ion. When an ion enters the chemisorption potential and moves outward along the outgoing trajectory, a substantial amount of the normal component of the kinetic energy will be dissipated via phonon and plasmon excitations, or electron–hole pair creation, on the surface. Reactive ions will have a large cross section in inelastic scattering, which leads to a substantial energy loss. In the scattering process, the normal and parallel components of energy are redistributed. Some of the ions scattered in the forward direction carry a small normal energy. If the normal energy of the ions is smaller than the potential barrier, they cannot escape and will be trapped moving parallel to the surface, as shown in Fig. 16(d). These ions can form a major portion of the reactive ions, because the energy loss will be quite large due to chemisorption interaction. Due to the loss of normal energy, the angular distribution will be narrow, with a portion of the large-angle scattering reduced because of the trajectory change. It is called skipping motion when an ion is reflected and returned to the surface several times.[37,38] The calculated energy spectra for scattered ions exhibit several discrete peaks that correspond to the number of surface collisions. In fact, Snowdon *et al.*[38] interpreted their study of (200–2000 eV)-Si^+-Cu(111) scattering under a grazing (1–14°) angle of incidence as evidence for this motion.

IV. SUMMARY

We have studied the scattering of O^+, O_2^+, C^+, CO^+, and CO_2^+ ions from a Pt(100) surface in a 10–400 eV energy range. The very low ion yields for oxygen ions were attributed to chemisorption interaction with the surface. The ion yields for CO^+ and CO_2^+ decreased steeply with increasing energy. The C^+ ion yield increased by one order of magnitude above 100 eV, and this increase was explained by reionization. Narrow lobes in the angular distributions were observed at 5–10° from the parallel to the surface below 100 eV. This indicates that surface trapping takes place and reduces the ion yield in large-angle scattering.

ACKNOWLEDGMENTS

We thank Professor K. Kuchitsu for critically reading the manuscript. This work was supported by the Grant-in-Aid for the Scientific Research from the Ministry of Education, Science and Culture.

[1] J. F. van der Veen, Surf. Sci. Rep. **5**, 199 (1985).
[2] D. F. Smith, J. Appl. Phys. **38**, 340 (1967).
[3] E. P. Th. M. Suurmeijer and A. L. Boers, Surf. Sci. **43**, 309 (1973).
[4] J. A. Baker and D. J. Auerbach, Surf. Sci. Rep. **4**, 1 (1985).
[5] M. P. D'Evelyn and R. J. Madix, Surf. Sci. Rep. **3**, 413 (1984).
[6] E. Kolodney, A. Amirav, R. Elber, and R. B. Gerber, Chem. Phys. Lett. **111**, 366 (1984).
[7] A. Danon and A. Amirav, Phys. Rev. Lett. **61**, 2961 (1988).
[8] B. Willerding, W. Heiland, and K. J. Snowdon, Phys. Rev. Lett. **53**, 2031 (1984).
[9] P. H. F. Reijnen, A. W. Kleyn, U. Imke, and K. J. Snowdon, Nucl. Instrum. Methods B **33**, 451 (1988).
[10] C. C. Chang, N. Winograd, and B. J. Garrison, Surf. Sci. **202**, 309 (1988).
[11] E. Hulpke and K. Mann, Surf. Sci. **133**, 171 (1983).
[12] A. D. Tenner, K. T. Gillen, T. C. M. Horn, J. Los, and A. W. Kleyn, Phys. Rev. Lett. **52**, 2183 (1984).
[13] A. Amirav and M. J. Cardillo, Phys. Rev. Lett. **57**, 2299 (1986).
[14] S. R. Kasi, M. A. Kilburn, H. Kang, J. Rabalais, L. Tavernini, and P. Hochmann, J. Chem. Phys. **88**, 5902 (1988).
[15] E. D. Fleischmann and J. E. Adams, Surf. Sci. **193**, 593 (1988).
[16] J. C. Tully, J. Chem. Phys. **73**, 6333 (1980).
[17] H. Nakatsuji, M. Hada, and T. Yonezawa, Surf. Sci. **185**, 319 (1987).
[18] H. Kang, S. Kasi, and J. W. Rabalais, J. Chem. Phys. **86**, 3753 (1987); H. Kang, S. R. Kasi, O. Grizzi, and J. W. Rabalais, J. Chem. Phys. **88**, 5894 (1988).
[19] H. Akazawa and Y. Murata, J. Chem. Phys. **88**, 3317 (1988).
[20] M. Menzinger and L. Wahlin, Rev. Sci. Instrum. **40**, 102 (1969).
[21] G. Kneringer and F. P. Netzer, Surf. Sci. **49**, 125 (1975).
[22] M. A. Barteau, E. I. Ko, and R. J. Madix, Surf. Sci. **102**, 99 (1981).
[23] H. Akazawa and Y. Murata, J. Chem. Phys. **92**, 5560(1990).
[24] H. D. Hagstrum, in *Inelatic Ion-Surface Collisions*, edited by N. H. Tolk, J. C. Tully, W. Heiland, and C. W. White (Plenum, New York, 1977).
[25] A. L. Boers, Nucl. Instrum. Methods B **4**, 98 (1984).
[26] L. K. Verhey, B. Poelsema, and A. L. Boers, Nucl. Instrum. Methods **132**, 565 (1976).
[27] C. E. Moore, *Atomic Energy Levels, NBS Circular 467* (National Bureau of Standards, Washington, DC, 1949, 1952, 1958), Vols. 1–3.
[28] K. P. Huber and G. Herzberg, *Molecular Spectra and Molecular Structure, Constants of Diatomic Molecules* (Van Nostrand Reinhold, New York, 1979), Vol. 4.
[29] N. V. Smith, G. K. Wertheim, S. Hufner, and M. M. Traum, Phys. Rev. B **10**, 3197 (1974).
[30] H. Akazawa and Y. Murata, Phys. Rev. Lett. **61**, 1218 (1988).
[31] H. Akazawa and Y. Murata, Phys. Rev. B **39**, 3449 (1989).
[32] S. Schubert, J. Neumann, U. Imke, K. J. Snowdon, P. Varga, and W. Heiland, Surf. Sci. **171**, L375 (1986).
[33] P. Haochang, T. C. M. Horn, and A. W. Kleyn, Phys. Rev. Lett. **57**, 3035 (1986).
[34] K. Saiki and S. Tanaka, Jpn. J. Appl. Phys. **21**, L329 (1982).
[35] R. Hentschke, K. J. Snowdon, P. Hertel, and W. Heiland, Surf. Sci. **173**, 565 (1986).
[36] K. J. Snowdon, Nucl. Instrum. Methods B **33**, 365 (1988).
[37] Y. H. Ohtsuki, K. Koyama, and Y. Yamamura, Phys. Rev. B **20**, 5044 (1979).
[38] K. J. Snowdon, D. J. O'Connor, and R. J. MacDonald, Appl. Phys. A **47**, 83 (1988); Phys. Rev. Lett. **61**, 1760 (1988).